Journal of Applied Polymer Science

Structure effect of thin film polypropylene view by dielectric spectroscopy and X-ray diffraction: Application to dry type power capacitors

Abdelkader Kahouli,[1,2] Olivier Gallot-Lavallée,[1,2] Pascal Rain,[1,2] Olivier Lesaint,[1,2] Laurent Heux,[3,4] Christophe Guillermin,[5] Jean-Marc Lupin[5]

[1]Univ. Grenoble Alpes, G2Elab, F-38000 Grenoble, France
[2]CNRS, G2Elab, F-38000 Grenoble, France
[3]University of Grenoble Alpes, CERMAV, F-38000 Grenoble, France
[4]CNRS, CERMAV, F-38000 Grenoble, France
[5]Schneider Electric, Rectiphase, F-74370 Pringy, France
Correspondence to: O. Gallot-Lavallée (E-mail: olivier.gallot-lavallee@g2elab.grenoble-inp.fr)

ABSTRACT: This work reports on the relationship between structure and dielectric properties of biaxially oriented polypropylene. The morphology of semicrystalline bioriented isotactic polypropylene films is investigated using wide angle X-ray diffraction and Polarized Optical Microscopy. A β-orthorhombic structure, with a crystallinity ratio of about 46%, and "Crater" morphology of the β-form is identified. Dielectric properties are measured by Broadband Dielectric Spectroscopy over a wide temperature range (-150 to 125°C). Since the dissipation factor of the PP is very low, special care was taken to obtain valid data. Two main relaxation processes are observed: a α-relaxation peak associated to the glass transition temperature (Tg) at temperature about -7°C, and a broad β^*-relaxation at about -60°C, partly attributed to CH orientation. The variation of the dissipation factor versus sample thickness (from 3.8 to 11.8 μm) is correlated and partly explained by the increase of crystallinity ratio and lamella size at larger thicknesses. It comes out that the thinnest film seems perfectly meet the application requesting, namely lowest dissipation factor and highest permittivity. © 2015 Wiley Periodicals, Inc. J. Appl. Polym. Sci. **2015**, *132*, 42602.

KEYWORDS: applications; dielectric properties; microscopy; spectroscopy; structure-property relations

Received 1 December 2014; accepted 7 June 2015
DOI: 10.1002/app.42602

INTRODUCTION

The application referred to in the background of this study concerns the power capacitor; the ones notably used to adjust the power factor (i.e., by reducing the phase shift between current and voltage), which result in significant savings of energy across the electric generation and transmission (typically about 10%; Figure 1).

The dielectric film, which is in the heart of to this study, is the main element of this capacitor (Figure 2). These metallized thin films are dedicated to the dry capacitor technology. The metallization of films have the main advantage to enhance a self-healing phenomenon. Indeed, the thin layer of metallization is sputtered by the thermal effect resulting from a local breakdown, which has benefic consequence to electrically insulate the localized default. In part against, the metallization thickness is necessarily low to allow this phenomenon (~10 nm) and hence, induces greater losses by series resistance. Thus best films are those which the capacity during time of running,[1] the sheet resistance of the metallization layer and the dissipation factor ($\tan \delta$), will be minimized. All this specifications must therefore lead to a better thermal stability of these capacitors.[2]

Among all existing polypropylene types, biaxially oriented isotactic polypropylene (BOiPP) is the preferable material for capacitors compared to unoriented PP films, due to its excellent electrical and mechanical properties, and better compatibility with synthetic insulating liquids.[3–6] Biaxially oriented PP can withstand three times the voltage of unoriented films, and also have a higher Young modulus.[7] These films are usually highly isotactic and crystalline, because of the steric regularity of CH_3 groups.

In this article, we investigated the morphology of films of three different thicknesses, together with their dielectric properties over a wide range of temperature and frequency, with the objective to analyze the relationship between these properties. The

Figure 1. Power capacitors based on films of this study, are used to improve the energy efficiency of electrical networks by minimizing the phase shift $\varphi_{(V/I)}$. Note that the angle δ involved in dissipation factor (tan δ) is egal to $(\pi/2)$-φ. [Color figure can be viewed in the online issue, which is available at wileyonlinelibrary.com.]

film structure and properties have been investigated thanks to Wide Angle X-ray Diffraction (WAXD), Polarized Optical Microscopy (POM), and Dielectric Spectroscopy (DS).

EXPERIMENTAL

Sample Properties

The studied PP is biaxially oriented. The starter process provides film samples stretched in two directions: the film is first stretched in machine direction then in transverse direction in accordance with a Stenter process.

The initial industrial metallization is done with an evaporated aluminum layer (thickness about 10 nm). The metallized surface is smoother than the other side (roughness, respectively, of 0.08 and 0.14 μm). The chemical structure of isotactic PP (iPP) is shown in Figure 3.

Three different film thicknesses were scrutinized: 3.8, 7.8, and 11.8 μm. These thicknesses were achieved by acting on the stretching parameters during Stenter process. Several measured film properties are summarized hereafter. Melting point: 167°C (DSC), Molecular weight of repeat unit: 42.08 g/mol, crystallinity ratio: $X_C = 46\%$ (DSC and WAXD), DC dielectric strength: 620 V/μm at room temperature for a 11.8 μm thickness).[8]

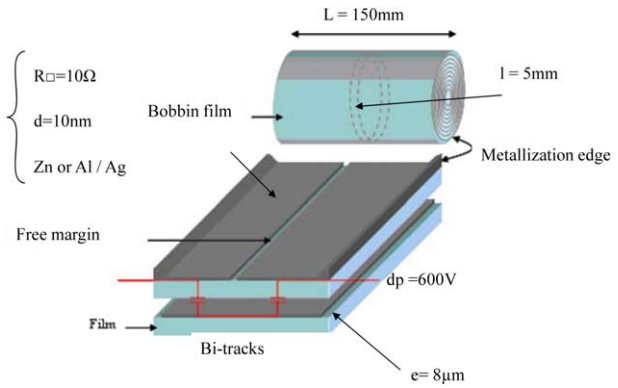

Figure 2. Typical architecture of dried power capacitors based on thin metalized films. According to applications, main specifications are $\Delta C(t_f)/C(t_0)<10\%$ (t_f and t_0 stand, respectively, for final and initial time of usage), minimize tan $\delta < 10^{-4}$, minimize serial resistance Ω□. [Color figure can be viewed in the online issue, which is available at wileyonlinelibrary.com.]

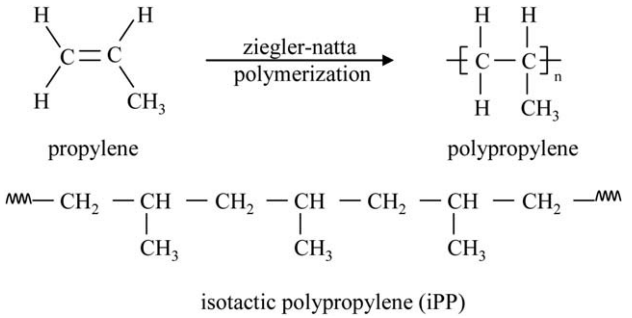

Figure 3. Chemical structures of propylene, polypropylene, and isotactic polypropylene (iPP).

Figure 4 shows the micrograph of 11.8 μm thick film. The observation shows a repeating pattern on the sample surface, corresponding to the micromorphology of the crystalline phase. These observations show the same "Crater" pattern as described in,[9] repeated with a random distribution with an average size varying from 100 to 250 μm.[9] The "Crater" is the main morphology associated to the crystalline form of BOiPP samples of the β-form, which show a birefringence character due to the presence of two related colors (blue and yellow) for each crystalline pattern (Figure 5).

Dielectric Analyzer Setup

Dielectric measurements were performed with a Novocontrol alpha A-high resolution (Figure 6).[10] It allows to measure complex impedance (Z^*) from which dielectrics properties such as relative permittivity (ε') and dissipation factor (tan δ) can be deduced. This device is necessary to achieve measurement on low loss materials such as PP. The theoretical absolute error on tan δ is 0.01% of measure $+3.5 \times 10^{-5}$ provided that C is between 80 pF and 8 nF. Figure 7 shows the experimental tan δ detection limit by an air capacitance.

Sample Conditioning

To obtain a proper electrical contact with the film, samples were metallized on both sides by evaporation of a silver layer, 30 nm in thickness. This was also done on the side already metallized with aluminum, to reduce the metallization surface resistance, and favor the connection with the measurement system (it was difficult to obtain a proper contact in the case of aluminum, due to the presence of an oxidation layer). The evaporation was made by Joule effect under a vacuum of 5.10^{-5} Torr. Particular attention was paid to limit the IR heating of the sample during this process. Samples were then placed between massive flat electrodes, and annealed at 100°C for 1 h under nitrogen in short-circuit conditions, to erase the previous sample "history" (mechanical constraints, space charges, etc.; Figure 8). Then they were slowly cooled down to room temperature. This protocol ensured a rather good reproducibility of measurements. Before this treatment, effect of serial resistance due to bad contact is observable at high frequency by the +1 slope (i.e., tan $\delta = RC\omega$). We increase by this treatment the surface of contact between the solid electrodes and the metallized surface of the film.

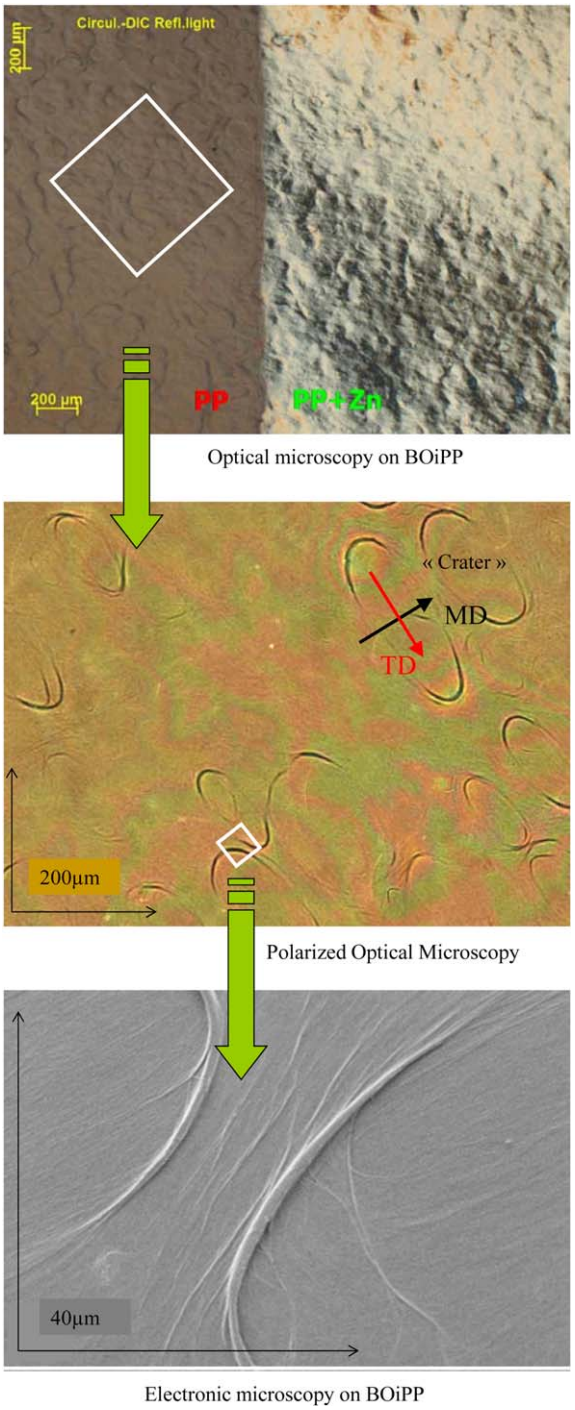

Figure 4. Micrograph of 11.8 µm thick BOiPP film. [Color figure can be viewed in the online issue, which is available at wileyonlinelibrary.com.]

RESULTS AND DISCUSSION

Crystallinity Analyses

The configuration and conformational states of the polypropylene chains influence the crystallization and the crystals form within the material. The isotactic polypropylene can crystallize into three different crystal forms depending on the temperature, pressure, and mechanical strains: monoclinic α-, hexagonal β-, and orthorhombic γ-forms.[11] The α-form is the most common

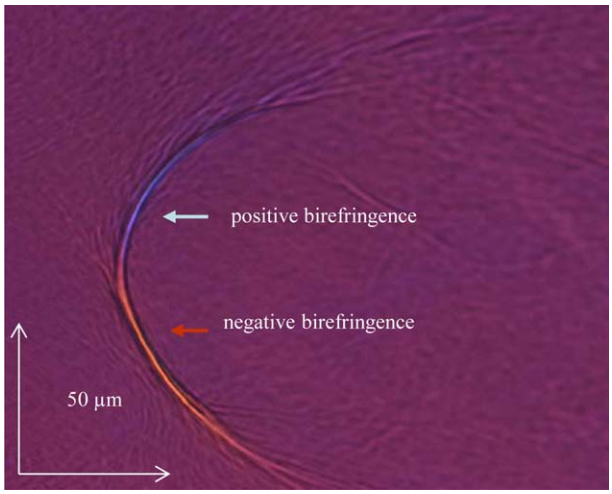

Figure 5. Birefringence of Crater morphology of 11.8 µm thickness of β-BOiPP. [Color figure can be viewed in the online issue, which is available at wileyonlinelibrary.com.]

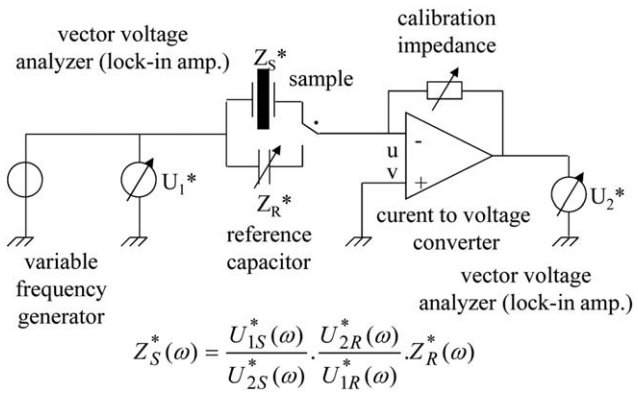

Figure 6. Electrical scheme and principle of dielectric analyzer: novocontrol alpha A high resolution.

structure. β-forms are found in systems crystallized under shear. The γ-crystals are formed only under high pressure with high molar mass polypropylene.[12–14]

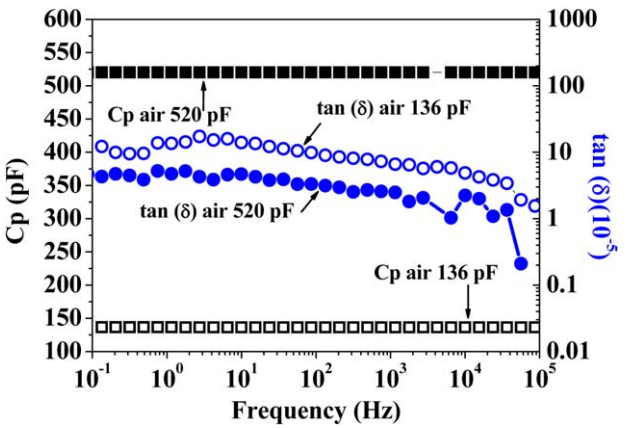

Figure 7. Dissipation factor versus frequency on air capacitor at two typical values of capacity, showing the experimental tan δ detection limit. [Color figure can be viewed in the online issue, which is available at wileyonlinelibrary.com.]

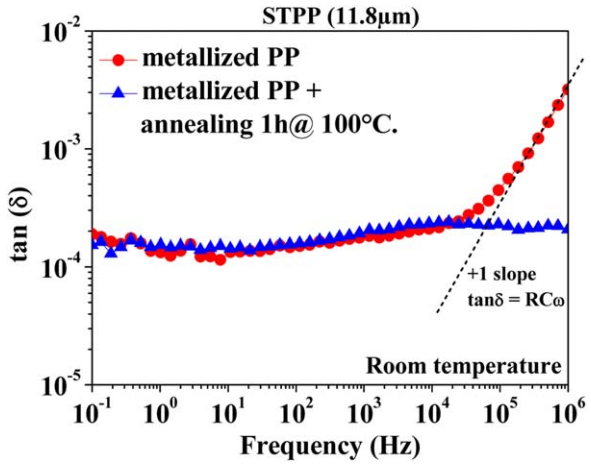

Figure 8. Dissipation factor versus frequency on a metallized PP before and after annealing treatment, which consisted in heating at 100°C for 1 h under nitrogen in short-circuit conditions. Before this treatment, effect of serial resistance due to bad contact is observable at high frequency; see tan $\delta = RC\omega$. [Color figure can be viewed in the online issue, which is available at wileyonlinelibrary.com.]

Figure 9 shows the WAXD patterns of BOiPP for film thicknesses of 3.8, 7.8, and 11.8 µm. According to the theoretical fit, the PP material shows a crystalline phase corresponding to the β-hexagonal ($a = 14.61$, $b = 14.61$, $c = 11.55$, and $\alpha = \beta = 90°$, $\gamma = 120°$) with (110), (301), (040), (130), and (400) orientations. The structure parameters of the β-form are quantified as shown in Table I. and imaged on Figure 10. This BOiPP film is composed of three phases. A crystalline phase in which the stresses are highest, a mobile amorphous phase in which the free volume is greater and the stresses are less important, and a rigid amorphous phase assuring the transition between the highly ordered crystalline phase and the mobile amorphous phase very disorderly. In this phase, the level of stress and order are slightly lower. Considering that typical thickness of the crystalline and amorphous regions in semicrystalline polymers are about 10 nm, we see that the interphase (1 nm size), constitutes

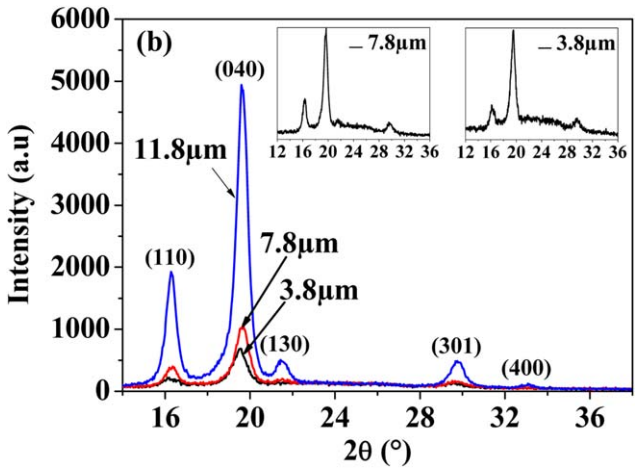

Figure 9. XRD-patterns of BOiPP according to sample thickness with a maximum penetration depth of about 20 nm. [Color figure can be viewed in the online issue, which is available at wileyonlinelibrary.com.]

Table I. Structural Data Calculated from WAXD Patterns (11.8 µm BOiPP Samples)

Reflexion peaks	2θ (°)	Interplanar d-spacing (Å)	Lamellae size Δ (nm)
(110)	16.31	6.31	17.1
(040)	19.64	5.24	15.2
(130)	21.50	4.79	15.6
(301)	29.77	3.48	14
(400)	33.08	3.14	24.2

an appreciable portion of the system volume and will consequently make a significant contribution to the macroscopic properties. Finally, note that all this three phases would relax differently.

For the thicker film (11.8 µm), five reflections with different orientations are seen, while for 7.8 and 3.8 µm films the orientations peaks (400) and (130) are absent or undetectable (see insets on Figure 9). Hence, the number of reflection peaks depends on the film thickness.[12–14]

The increase of the lamellae size is evidenced by the decrease of the full width at half maximum (FWHM) of the (040) reflection as the film thickness increases. The lamellae size Δ is computed using the Debye-Scherrer eq. (1):

$$\Delta = \frac{K\lambda}{\mathrm{FWHM}\cos(\theta)} \quad (1)$$

where K is a proportionality constant ~0.9, FWHM the full width at half maximum, θ the diffraction angle and λ the wavelength of the cobalt source ($\lambda = 1.79$ Å). For this 040 diffraction peak, calculations showed that the lamellae size Δ increases with the film thickness: $\Delta = 11.9$, 12.9, and 15.2 nm, respectively, for 3.8, 7.8, and 11.8 µm thicknesses. However, since the diffraction position is similar for 7.8 and 11.8 µm, the d-spacing remains constant according to the Bragg eq. (2):

$$2d\sin(\theta) = n\lambda \quad (2)$$

where n is the number of the diffraction plans having the same reflexion (040).

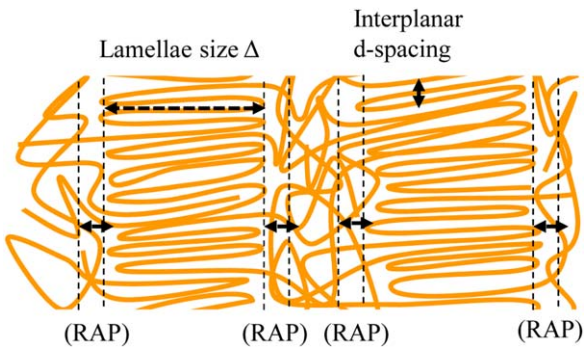

Figure 10. Representation of a semicrystalline structure with designation of lamellae, interplanar, and rigid amorphous phase (RAP). [Color figure can be viewed in the online issue, which is available at wileyonlinelibrary.com.]

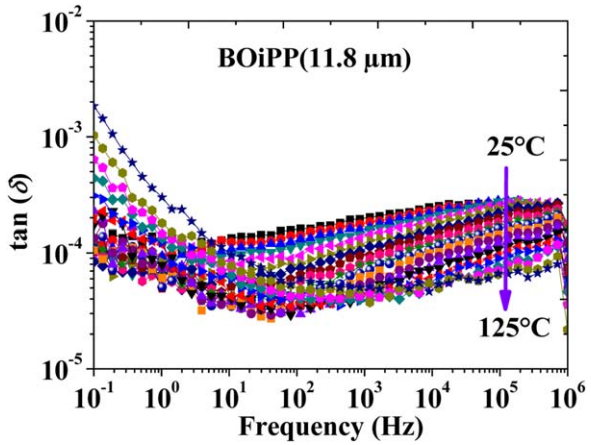

Figure 11. Dissipation factor versus frequency at different temperatures from 25 to 125°C (isothermals curves). Film thickness: 11.8 µm. [Color figure can be viewed in the online issue, which is available at wileyonlinelibrary.com.]

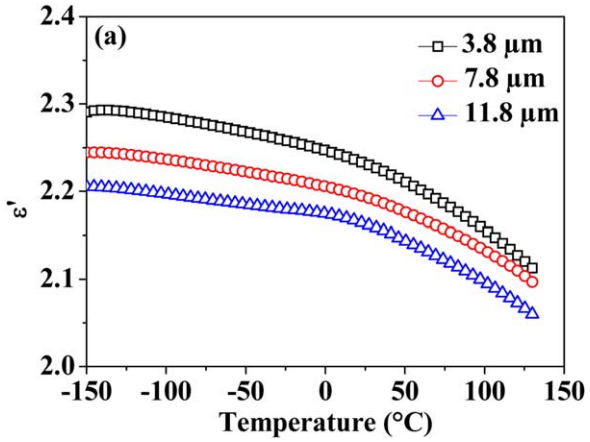

Figure 12. Dielectric constant of BOiPP at 70 Hz versus temperature for different film thicknesses (from isothermals curves). Thickness is given with a tolerance of 0.52%. [Color figure can be viewed in the online issue, which is available at wileyonlinelibrary.com.]

Finally, the more intense diffraction peaks reveal that the crystallinity ratio increases with thickness.

DS Analyses

The dielectric response is generally described by the complex permittivity $\varepsilon^* = \varepsilon' - i\varepsilon''$, where real ($\varepsilon'$) and imaginary ($\varepsilon''$) components represent the storage and loss of energy in each cycle of applied electric field.

Figure 11 shows the overall behavior of the dissipation factor tan $\delta = \varepsilon''/\varepsilon'$ versus frequency, at temperatures from 20 to 125°C. The dissipation factor exhibits low values, between 10^{-4} and 2.10^{-4} at room temperature over the whole frequency range investigated (10^{-1}–10^{6} Hz), and down to 3.10^{-5} at higher temperatures. Since these values are quite close to the intrinsic limits of the measurement system, a great attention was paid to optimizing the measurement conditions, and to checking the validity of measurements.

For frequencies above a few Hz, a decrease of tan δ is observed when temperature is increased up to about 90°C. This confirms that BOiPP is a very good material to build ac power capacitors. Indeed, the decrease of losses versus temperature greatly contributes to the temperature stability of capacitors, provided the temperature remains lower than typically 90°C. A reversed tendency (increase of tan δ versus temperature) is observed at higher temperatures (>95°C), at frequencies below typically 100 Hz. The lowest the frequency, the largest the tan δ increases. At 50 Hz, tan δ at 125°C remains lower than the value measured at 20°C, whereas at 10^{-1} Hz, it increases by one decade. This large increase can be attributed to the influence of the ionic conduction at high temperatures.[8]

Outside this high temperature range, tan δ shows a moderate spread, that is, weak relaxation phenomena are present. In the frequency range investigated, ε' is perfectly stable versus frequency. It decreases slightly with temperature: for a 11.8 µm thickness, the permittivity decreases from 2.2 at 25°C down to 2.05 at 125°C (i.e., −7%/100°C; Figure 12). Although a minor part is due to the thermal expansion approaching 1%/100°C. Note finally that these values are also slightly decreasing with the increase of film thickness.

Figure 13 shows the plot of the dissipation factor versus temperature for different frequencies. The presence of two relaxation processes can be seen. They are shifted toward higher temperatures when the frequency increases. The first relaxation process appears in the temperature range (−75 to −20°C), as a broad peak in tan δ. This peak can be attributed to the β^*-relaxation, as observed in semicrystalline poly(ethylene 2,6-naphthalene dicarboxylate) biaxially stretched films (25 µm thickness).[15]

As the temperature increases, we can see the occurrence of a second relaxation peak (−20 to 0°C range). This α peak is associated to the glass transition of the material, occurring in the mobile amorphous phase. The glass transition temperature *Tg* of the 11.8 µm film, measured at the peak α of tan δ at 1 Hz, is about −12°C, in good agreement with the value measured by differential scanning calorimetry (−6°C).[16–18]

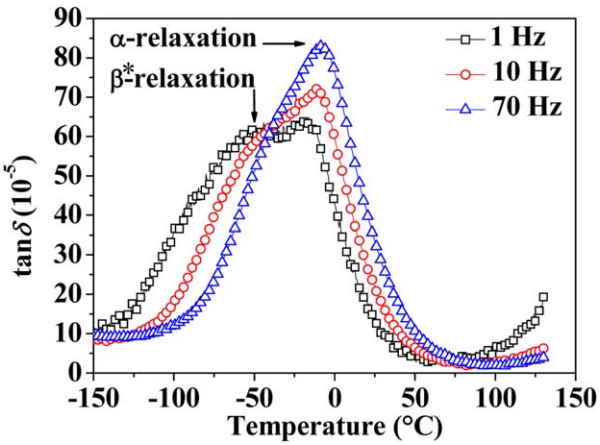

Figure 13. Dissipation factor versus temperature at different frequencies; film thickness: 11.8 µm; *Cp* = 520 pF (from isothermals curves). [Color figure can be viewed in the online issue, which is available at wileyonlinelibrary.com.]

Figure 14 shows the dissipation factor of another grade of BOiPP at 70 Hz versus temperature for different film thicknesses. It can be observed that the dissipation factor increases sharply with the thickness. Furthermore, the relative magnitude of the α-relaxation seems to decrease in comparison to the β^*-peak. Concede that the quantitative difference observed in the three grades of thickness is only significant around the glass transition temperature as it should be borne in mind that this low level of losses is easily affected up to 5.10^{-5} by a change of capacitance.

Figure 15 shows the variation of the peak frequency *fmax* of relaxations processes versus the inverse of temperature for different film thicknesses. The peak frequency of the α-relaxation obeys to the empirical Vogel–Fulcher–Tammann law (VFT) eq. (1), where A is a constant, T_o is the temperature at which molecular mobility is freeze which can be also associated to the VFT temperature and E_a is the activation energy of the relaxation process. This fit confirms that this α-relaxation process is linked with the glass transition of this grade of BOiPP.

$$f(T) = A \exp\left(-\frac{E_a}{T - T_0}\right) \quad (3)$$

The maximum frequency of the β^* relaxation obeys to an Arrhenius law. It appears that the increase of film thickness causes a decrease of the apparent activation energy E_a. The values of E_a (>1 eV) for the three film thicknesses suggest that the relaxation observed at low temperature is not governed by local motion, but rather by partially cooperative motions. Note that it is known that the activation energy for the β^*-process is higher than the value obtained for the β-relaxation (associated to local motion).[16,19–21]

The thickness is essentially a technical aspect to produce a film consisting in acting on the temperature and stretching parameters. This realization parameter seems to produce several effects including effects on the microstructure. It is also observed that the lamellas size and the crystallinity ratio, increase with the thickness (Figure 9 and Table I). The rigid amorphous phase therefore increases compared to the mobile amorphous phase (Figure 10). But how to explain on this basis the increase of dissipation factor and the reducing of relative permittivity. To answer this question, we propose here to make an analogy with the behavior of polyethylene with more or less high density (i.e., with a variable ratio of crystallinity). In the case of high density polyethylene, the dissipation peak, which is due to local motion (alpha peak in their case and beta peak in our case), is largely due to the relatively constraint phase such as the crystalline phase and the rigid amorphous phase. At the same time, the share of mobile amorphous polymer and more overall the free motion having reduced, consequently the relative permittivity decreases. In this situation, de involved group in motion could come from CH group.[3] But, this scenario is probably too simple to account for all the complexity of the mechanisms involved in the spectral signature of the PP. Recall for example, that increasing the thickness, decreases the ratio of oxidation relative to the volume of the film. However, these materials which are non-polar, are from point of view of the DS, deemed very sensitive to the appearance of carbonyl group. According Schönhals *et al.*,[22,23] the interdependence that exists between the mobile amorphous regions, amorphous, and crystalline rigid, never totally exclude any of the three phase to the final signing of the dielectric spectrum.

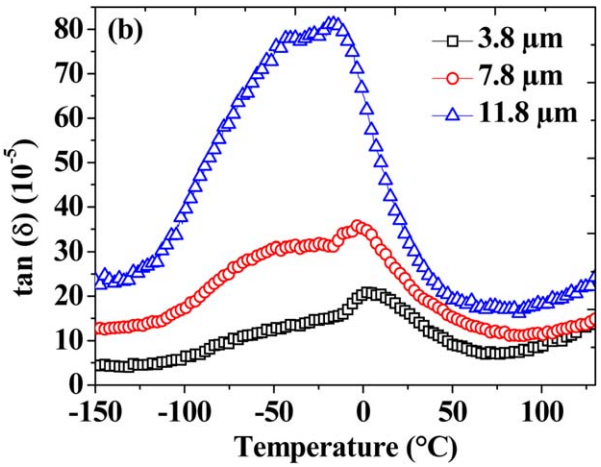

Figure 14. Dissipation factor of BOiPP at 70 Hz versus temperature for different film thicknesses; $Cp = 520$ pF (from isothermals curves). [Color figure can be viewed in the online issue, which is available at wileyonlinelibrary.com.]

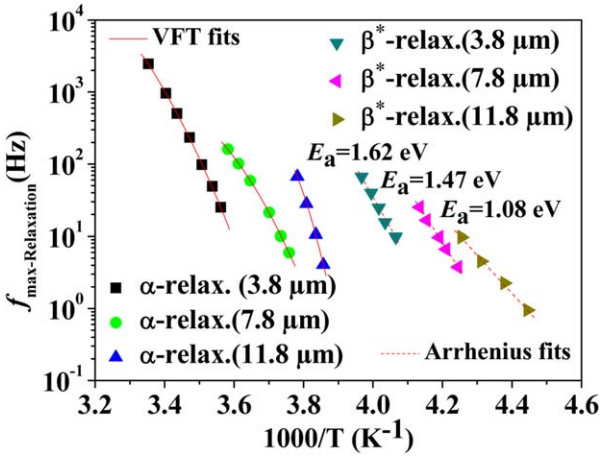

Figure 15. VFT and Arrhenius fits of relaxation processes occurring in BOiPP films; $Cp = 520$ pF. [Color figure can be viewed in the online issue, which is available at wileyonlinelibrary.com.]

SYNTHESIS

WAXD reveals that the biaxially oriented isotactic polypropylene (BOiPP) is in the β-form (Orthorhombic system), and that the crystallinity ratio increases with the film thickness. A "Crater" morphology with an average size between 100 and 250 µm has been observed by POM.

The dielectric properties of BOiPP films were characterized in the frequency range 0.1Hz - 1 MHz over a wide temperature range from −150 to 130°C. Thanks to DS, two main relaxation peaks have been identified: β^* (around −60°C) and α (around −7°C). The β^* relaxation is partly attributed to the orientation of CH group. The maximum frequency of this peak obeys to an

Arrhenius law, with an activation energy increasing from 1.08 eV to 1.62 when the crystalinity as lamella size decreases via the film thickness from 11.8 to 3.8 μm. The α relaxation is associated to the glass transition (*Tg*) of the material, occurring in the mobile amorphous phase.

BOiPP films show very low losses with a minimum around 90°C at 70 Hz, and a variation with temperature favorable for their application in ac power capacitors. The dielectric properties of PP films depend on their thickness, in correlation with the observed variations of the film structure (larger crystallinity ratio in thicker films). The thinnest film seems perfectly meet the application requesting, namely lowest dissipation factor and highest permittivity.

ACKNOWLEDGMENTS

Thanks to Rhone Alpes Region, which funded this project through the cluster TENERRDIS.

REFERENCES

1. Kahouli, A.; Lesaint, O.; Gallot-Lavallée, O.; Rain, P.; Guillermin, C. A study of factors and mechanisms responsible for the de-metallization of polypropylene films used in dry capacitors. Proceeding of CEIDP, Montreal, IEEE, **2012**; p 688.
2. Gallot-Lavallée, O. Dielectric Materials and Electrostatics; John Wiley & Sons Inc.: Hoboken, NJ, **2013**; p 1.
3. Umemura, T.; Akiyama, K.; Couderc, D. *IEEE Trans. Elec. Insulation.* **1986**, *21*, 137.
4. Zhuravlev, S. P.; Zhuravleva, N. M.; Polonskij, Y. A. *Russ. Electr. Eng.* **2002**, *73*, 52.
5. Fournie, R. *Bull. Direction Études Recherches* **1990**, *1*, 1.
6. Barshaw, E. J.; White, J.; Chait, M. J.; Cornette, J. B.; Bustamante, J.; Folli, F.; Biltchick, D.; Rabuffi, M. *IEEE Trans. Magn.* **2007**, *43* 223.
7. Vaughan, A. S.; Zhao, Y.; Barré, L. L.; Sutton, S. J.; Swingler, S. G. *Eur. Polym. J.* **2003**, *39*, 355.
8. Kahouli, A.; Gallot-Lavallée, O.; Rain, P.; Lesaint, O.; Guillermin, C.; Lupin, J. M. A comparison of electric and dielectric properties of standard and high-crystallinity polypropylene films. *Proc. ICSD, Bologna, IEEE* **2013**; p 23.
9. Tamura, S.; Takino, K.; Yamada, T.; Kanai, T. *J. Appl. Polym. Sci.* **2012**, *126*, E501.
10. Schaumburg, G. Overview: Modern measurement techniques in Broadband Dielectric Spectroscopy, *Novocontrol-Dielectrics Newsletter* **1994**; p 4.
11. Bruckner, S.; Meille, S. V.; Petraccone, V.; Pirozzi, B. *Prog. Polym. Sci.* **1991**, *16*, 361.
12. Addink, E. J.; Beintema, J. *Polymer* **1961**, *2*, 185.
13. Turner-Jones, A.; Aizlewood, J. M.; Beckett, D. R. *Makromilek. Chem.* **1964**, *75*, 134.
14. Nagasawa, S.; Fujimori, A.; Masuko, T.; Iguchi, M. *Polymer* **2005**, *46*, 5241.
15. Hardy, L.; Stevenson, I.; Fritz, A.; Boiteux, G.; Seytre, G.; Schönhals, A. *Polymer* **2003**, *44*, 4311.
16. Androsch, R.; Di Lorenzo, M. L.; Schick, C.; Wunderlich, B. *Polymer* **2010**, *51*, 4639.
17. Botev, M.; Neffati, R.; Rault, J. *Polymer* **1999**, *40*, 5227.
18. Gracias, D. H.; Zhang, D.; Lianos, L.; Ibach, W.; Shen, Y. R.; Somorjai, G. A. *Chem. Phys.* **1999**, *245*, 277.
19. Stauga, R.; Schönhals, A.; Carius, H. E.; Mudrak, C. V.; Privalko, V. P. *New Polym. Mater.* **1998**, *5*, 119.
20. Prabu, A. A.; Kim, K. J.; Park, C. *Vib. Spectrosc.* **2009**, *49*, 101.
21. Liang, T.; Makita, Y.; Kimura, S. *Polymer* **2001**, *42*, 4867.
22. Kremer, F.; Schönhals, A. Broadband Dielectric Spectroscopy; Springer Science & Business Media: Berlin, Heidelberg, **2003**.
23. Runt, J.; Fitzgerald, J. Dielectric spectroscopy of polymeric materials; American Chemical Society: USA, **1997**.